Electronic Supplementary Information

Co-assembly of Structurally Different Biomacromolecules-modified Maghemite Nanoparticles with Nitrate Sequestration Potential

Hui Dong[a], Bo Su[a, b], YanXi Cheng[a], Saikat Ghosh[a*], Nihar R. Pradhan[c], Bo Pan[a] and Baoshan Xing[d]

[a]Kunming University of Science and Technology, Kunming, China 650500

[b]Ecological Environment Geo-Service Center of Henan Geological Bureau, Zhengzhou 450053, China

[c]Department of Chemistry, Physics & Atmospheric Science, Jackson State University, Jackson, Mississippi 39217, USA

[c] Stockbridge School of Agriculture, University of Massachusetts, Amherst, Massachusetts 01003, United States

*Corresponding Author's E-mail: saikatgh.1970@gmail.com (Saikat Ghosh)

Methods

Preparation of BSA- and HA-coated γFe_2O_3 NPs suspensions

BSA-coated γFe_2O_3 NPs (B-GFeNPs) were prepared by mixing 1 g γFe_2O_3 NPs (G-FeNPs) in 100 ml. BSA (500 mg/L) solution at pH 4. Similarly, HA-coated γFe_2O_3 NPs were prepared by mixing 1 g γFe_2O_3 NPs in 100 ml 500 mg/L HA solution at pH 4. The BSA/HA and G-FeNPs mixture was put into a rotary shaker (100 rpm) for three days at 25°C. The pH of the mixture was adjusted to pH 4 every 24 hrs. with 0.1 M HCl/0.1 M NaOH. After the complexation reaction, the mixture was centrifuged at 20000 rpm at 4°C for 15 minutes, followed by total organic carbon (TOC) measurement (Vario TOC, Elementar Co., Germany). This process has been repeated seven times till the TOC content of the supernatant diminished to that of deionized water. The produced complexes were then stored in a refrigerator. The particle concentration in the suspensions was measured after determining Fe concentrations using an atomic absorption spectrophotometer (Z-2000, Hitachi, Japan).

Circular Dichroism Spectroscopy (CD)

The conformational alterations of BSA in the absence and presence of GFeNPs were determined using a BRIGHTTIME Chirascan CD spectrometer (Applied Photophysics Ltd., Leatherhead, UK), according to the method proposed by Li et al (2015).[1] The roles of solution pH and $NaNO_3$ on the conformational alterations of BSA and B-GFeNPs were determined from the CD spectra of suspensions containing a mixture of BSA (8×10^{-6} M) and GFeNPs (10 mg/L). The conformation changes of the BSA–GFeNP mixture were assessed in the presence of 1 and 10 mM of $NaNO_3$ and 50 mg/L of HA. CD spectra were collected within 190–260 nm using a 0.5-mm path length.

Three-dimensional Excitation–Emission Matrix Fluorescence Spectra (3DEEM)

The 3D-EEM spectra of BSA, HA, and the mixtures were measured at wavelength ranges of 200–550 nm (excitation) and 250–550 nm (emission) at a scanning speed of 2400 nm/min at pH 4 and 7 in the presence and absence of 10 mM $NaNO_3$. The suspension concentrations were maintained at 10 mg C/L using an F-4500 fluorescence spectrometer (Hitachi, Tokyo, Japan). The spectra were plotted using Origin software.

Determination of radius of gyration (R_g) and conformation of the protein in a solution with SAXS and XRD investigation of the colloidal crystals

Sample solutions were put in quartz capillary tubes (Internal Diameter (ID) 1.6 mm) equipped with a collection adapter (ID 1.5 mm). The SAXS experiment is based on elastic scattering of X-rays, where a sample solution including 100g/L BSA, and 100g/L BSA in 1M $NaNO_3$ was placed in capillary tubes and exposed to the focused, monochromatic X-ray beam. SAXS data were collected as a function of the scattering vector following the equation:

$$q = \frac{4\pi}{\lambda} Sin\ \theta \text{.....(1)}$$

2θ is the scattering angle, λ is the wavelength of the incident X-ray. Guinier (1939) developed the scattering intensity analysis to determine zero angle scattering which directly falls within the beam-stopper shadow region to determine I_0, and the radius of gyration R_g i.e. root mean square (r.m.s.) distance from all its points to the center; since the highest scattered intensities come at the lowest angles with the assumption of negligible aggregation and inter-particle repulsion. A linear relationship between the Guinier plot obtained from the scattering intensity. The Guinier plots of the samples for small values of the scattering vector q and the determination of the radius of gyration (R_g) are obtained from the following equation[2]:

$$I_q = I_0.e^{-\left(\frac{q^2.R_g^2}{3}\right)} \quad \text{.....(2)}$$

deducing the mean scattering intensity of particles of diverse shapes upon their various spatial conformations in solution.[3] Factors like inadequate background subtraction, the presence of strong inter-particle interactions, and above all, high sample polydispersity will result in deviation from linearity.

Theory of ^1H spin-spin relaxation (R_2)

In a static magnetic field, magnetic moments of water precess at the Larmor frequency, which is proportional to the local magnetic field. The local magnetic field inhomogeneities created by the SPIONs with various surface modifiers cause nearby proton magnetic moments to precess at different rates, leading to an alteration in phase coherence. This dephasing of the ^1H proton spins provides the contrasting behavior of interparticle and solvent-particle interactions, both in B-GFeNPs and H-GFeNPs in aqueous medium. The pH-dependent alteration in colloidal stability is deduced from surface-modified NP's ^1H exchange with neighboring water molecules against a sufficiently strong static "Z"-directed external magnetic field. The colloidal stability of the suspensions derived from the mutual interactions between the inherent magnetic moments of NPs and the electrosteric contribution of the surface modifiers against destabilizing forces can be ascertained more critically from R_2 data. Nonetheless, the inherently higher accuracy of NMR techniques relative to light scattering-mediated average D_H further elucidates the difference in colloidal stability. The mathematical expression for the local magnetic inhomogeneity evolved from the cluster size variation in a uniform precessing magnetic field affecting the rate of relaxation is[3]:

$$B\ (r,\ \theta) = \frac{\mu_0 m}{4\pi}\left[\frac{3\ Cos^{\ 2}(\theta) - 1}{r^3}\right] \text{.....(3)}$$

Where B is the external magnetic field, r is the NP's radius, and m is the NP's magnetic moment pinned along the Z-direction. Since the external "Z"-directed magnetic field is sufficiently strong to overcome mutual interactions between NPs, r is the position of ^{1}H nuclei from the center of the magnetic field, θ is the angle with the Z-axis, and μ_0 is the permeability of the free space.

Experimental method: The Carr–Purcell–Meiboom–Gill (CPMG) pulse sequence of 200-600 echo cycles with 0.5 ms echo spacing (τ), and sequential application of 90º and 180º pulses of 8 μS and 17 μS durations, respectively.

Kelvin Probe Force Microscopy (KPFM) and Magnetic Force Microscopy (MFM)

KPFM measurements of the assembled structures were carried out upon adsorption of the colloidal mixtures in the presence of salt solutions on doped silicon wafer substrates cut into a square with sides 0.8 cm long. A 1:1 mixture of 20 mg/L suspensions of B-GFeNPs and H-GFeNPs in the presence of 10 mM and 100 mM $NaNO_3$ at pH 4 and pH 7 was adsorbed on the substrate surface for 20 min. The weakly adhered particles were then washed with the salt solutions, followed by drying under an N_2 atmosphere. Then conductive silver paint (SPI, USA) was used to stick the silicon wafers to ensure the electrical conductance of the samples attached to the sample stub. Each surface potential is obtained at AM-KPFM mode by Bruker Multimode 8 AFM (Bruker, Germany) with a lift scan height of 100 nm. An MESP-V2 (Bruker) with a spring constant of 3 N/m and a resonance frequency of 75 kHz was used for these experiments.

MFM measurements of ferrimagnetic γFe_2O_3 NPs (25−50 nm) (Nanoamor, Houston, TX, USA), and poly acrylic (PAA, 2000D, Polyscience) modified γFe_2O_3 NPs were carried out with a

45 nm Co/Cr magnetized MFM tip (MFM, Asylum Research, USA) at a constant lift height of 30 nm. The detailed experimental procedure regarding the preparation of PAA2K-coated γFe_2O_3 NPs and MFM measurements can be obtained from our earlier work.[4]

Scanning Electron Microscopy (SEM)

The samples were mounted on aluminum stubs using double-sided carbon tape gold gold-coated with a sputter coater. Samples were analyzed with a TESCAN, VEGA3 SBH, Czech Republic, equipped with an EDX Thermo Fisher Noran System 7, Thermo Fisher Scientific, Waltham, MA, USA.

X-ray diffraction (XRD)

X-ray diffraction patterns (XRD) of the assembled structures in the presence and absence of $NaNO_3$ were determined with a Rigaku Ultima IV (Japan) instrument. Briefly, a 10 mg/L 1:1 mixture of B-GFeNPs and H-GFeNPs in 10 mM $NaNO_3$ was freeze-dried, followed by suspending in deionized water and spreading onto a glass substrate, followed by XRD measurement.

Results and Discussions:

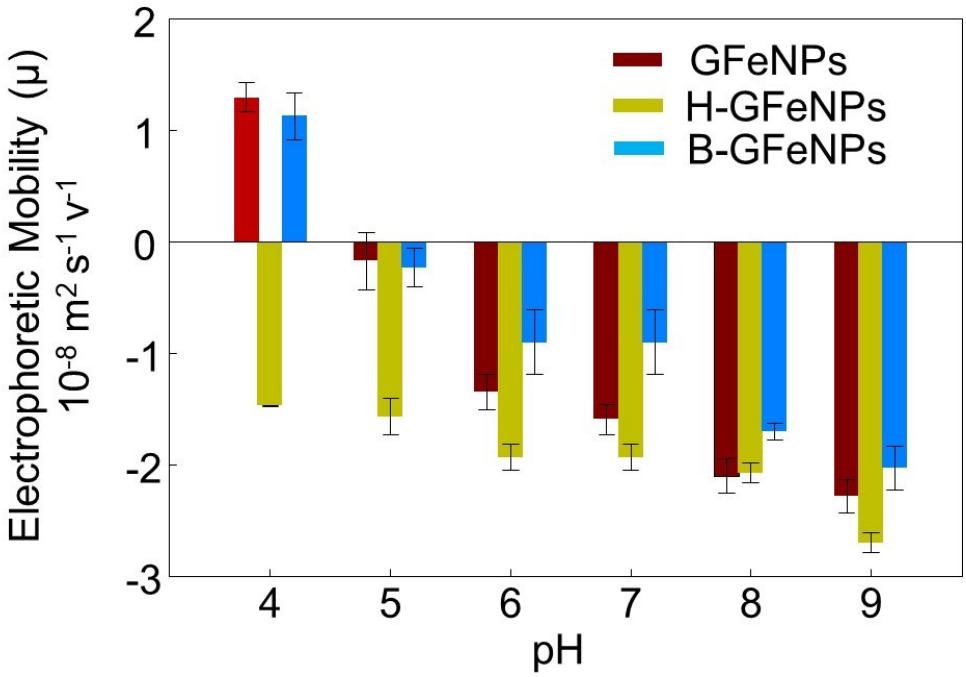

Figure S1. Electrophoretic mobility (μ) of G-FeNPs, B-GFeNPs, and H-GFeNPs in the range of environmentally relevant pHs. Sorption of HA on G-FeNPs at pH 4 showed overcharging of G-FeNPs due to the lower pK_a of ionized carboxylate ions abundant in HA.

MFM imaging of the ferrimagnetic γFe_2O_3 NPs and polyacrylic acid-coated γFe_2O_3 NPs

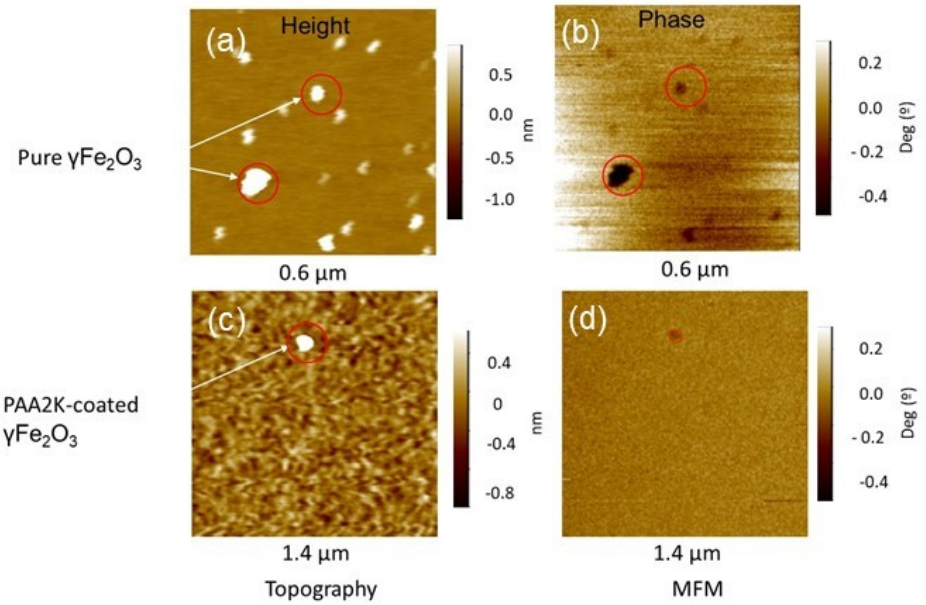

Figure S2. AFM height and MFM phase images of ferrimagnetic maghemite NPs (a) height and (b) magnetic phase with a lift scan height of 30 nm. (c and d) Surface modification of maghemite NPs with PAA 2K showed the loss of surface magnetic moments but the presence of core moments.

Conformation and specific interactions of biomolecules and anions adsorbed on the maghemite surface:

Neither unbound HA nor HA adsorbed on the NP surface exhibited preferred optical activity, possibly owing to their structural heterogeneity. However, BSA and B-GFeNPs showed characteristic CD absorption minima at ~208 nm (n–π*) and ~222 nm (π–π*), respectively, representing the α-helical structure. The CD spectra revealed that the adsorption of BSA on the NP surface did not cause substantial structural changes to BSA but altered its secondary structure (Figure 2). The α-helix percentage of BSA from the unbound to adsorbed state was reduced from 56% to 13% at pH 4 and 61% to 25% at pH 7, suggesting less loss of the BSA secondary structure

at higher pH. An earlier investigation reported that the binding of MnO_2 NPs with BSA did not denature the protein but altered its secondary structure, reaching a minimum with an enhanced proportion of MnO_2 NPs in the mixture.[5] Furthermore, environmentally relevant chaotropic NO_3^- can substantially influence the conformation of unbound and surface-bound protein biomolecules upon alteration of their secondary structure, hence influencing their colloidal interactions. Protein unfolding mechanisms mainly follow two pathways: interaction with β-sheets and/or α-helices. Previous studies have elucidated that urea unfolds the protein's secondary structure by acting upon β-sheets, whereas the guanidinium ion (Gd^+) interacts with the α-helix part of the protein.[6] The CD spectra of B-GFeNPs in the presence of 1 mM of NO_3^- revealed an increase in the α-helix component but a net loss in the presence of 10 mM of NO_3^-. This aligned with the observation that low Gd^+ concentrations caused an initial gain in the molar ellipticity of BSA but a net loss at higher concentrations.[6] The molar ellipticity or mean residue ellipticity (MRE) is calculated as follows:

$$MRE\left(deg\cdot cm^2\cdot dmol^{-1}\right) = \frac{\theta_{obs}\,(mdeg) \times M}{nlc} \quad (1)$$

where θ_{obs} is in millidegrees, M is the molecular weight of BSA in $g\cdot d\cdot mol^{-1}$, n is the number of amino acid residues (583 in the case of BSA), l is the path length (0.05 cm) of the cuvette, and c is the concentration of the protein in $g\cdot L^{-1}$. The results indicated that NO_3^- strongly altered the conformation of unbound and NP-bound proteins, corresponding with chaotropic ion-induced conformational changes (Figures S3–S5). Solvation of these anions with neighboring water molecules further determined their binding efficiency with protein biomolecules. Two-dimensional infrared (2D-IR), ultraviolet-visible–infrared (UV–Vis–IR), and UV–Vis time-resolved spectroscopies in combination with molecular dynamics simulations previously revealed that a highly labile hydration shell adhered to NO_3^- with weakened H bonding with neighboring water molecules in aqueous medium.[7] This aligned with the NO_3^--induced fluorescence quenching

of tryptophan (Trp) residues in BSA, indicating the presence of direct binding between NO_3^- with the positively charged amino acid residues and exposure to the polar environment, as shown by 3D-EFM (Figure S4). Gd^+-induced loss of the α-helical structure of BSA corroborated the fluorescence quenching of Trp residues upon exposure of the latter to a more polar bulk-like environment relative to their native state.[7] Moreover, Salvi et al. (2005) reported that the hydrophobic effect driving the foldability of protein biomolecules can be severely influenced by chaotropic hydrophobic hydration.[8] Thermodynamically, reduced interfacial contact between protein and surrounding water molecules, condensation, and crowding of chaotropic anions toward the hydrophobic domain can alter protein conformation.

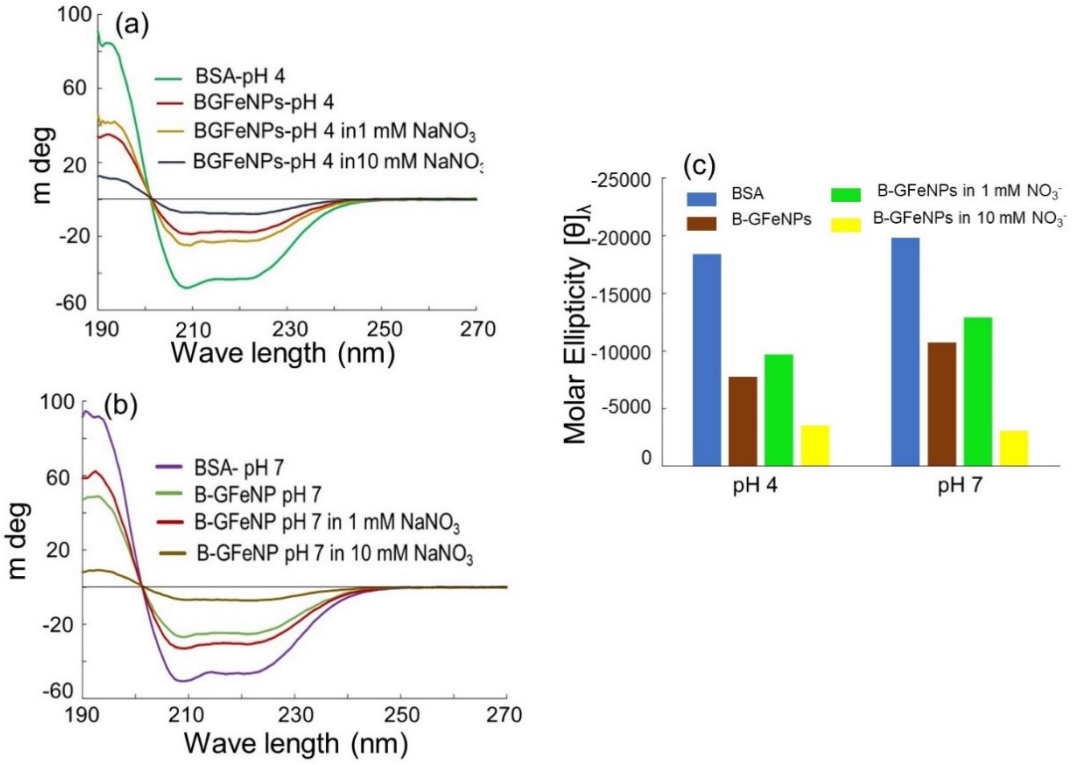

Figure S3. CD spectra of BSA and B-GFeNPs in the presence and absence of NO_3^- at (a) pH 4 and (b) at pH 7. BSA sorption on the NP surface and attenuation of chaotropic NO_3^- contribute to the loss of α-helicity, as observed from the characteristic absorption minima at 208 and 222 nm, respectively. Enhanced NO_3^- concentration contributed to the loss of α-helical structure at pH 4 and 7. (c) Comparison of the molar ellipticity (MRE) plots of B-GFeNP absorption at 222 nm at pH 4 and pH 7 in the presence of NO_3^-.

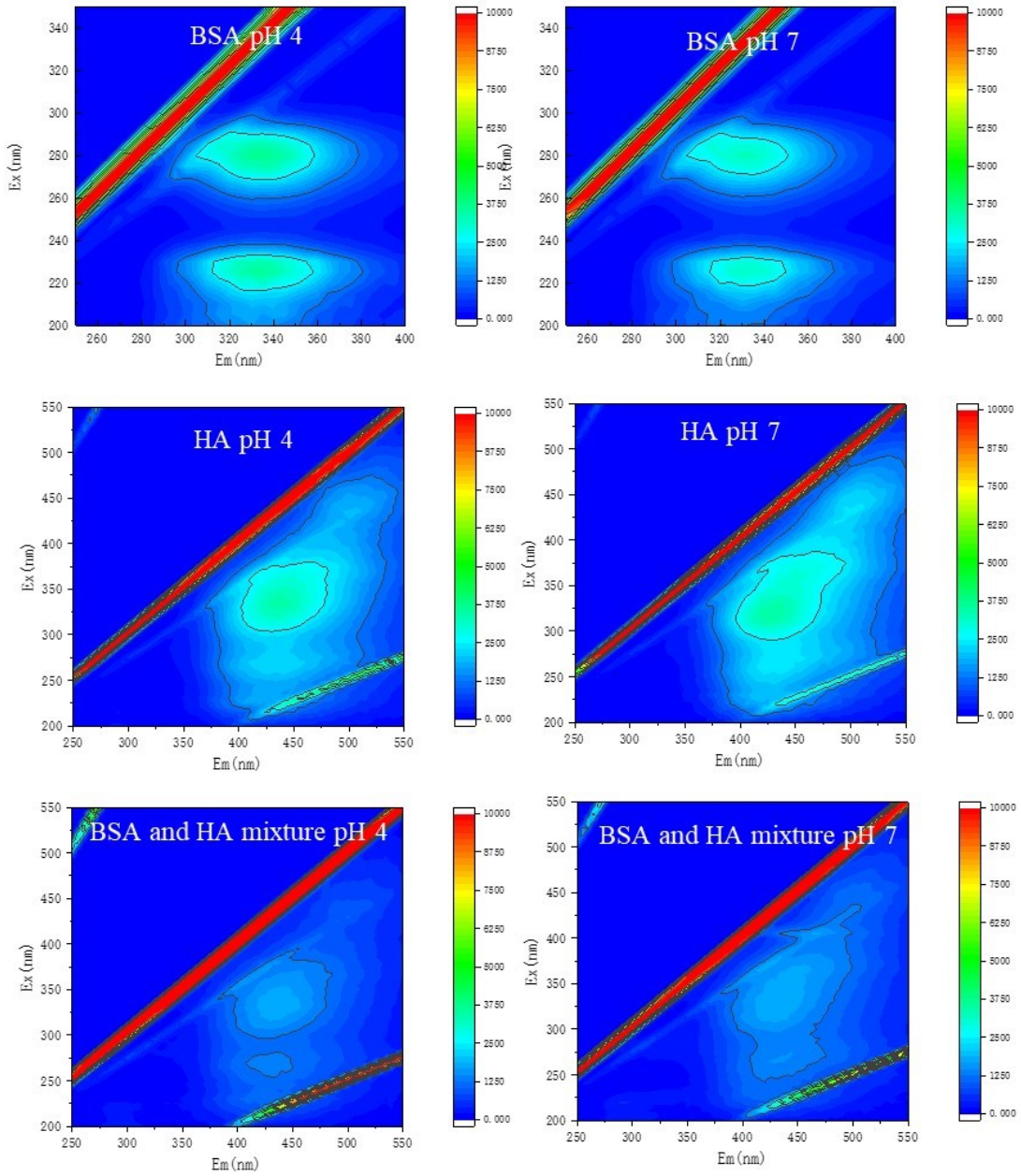

Figure S4. 3DEFM spectra of BSA, both at pH 4 and pH 7, exhibited two E_x/E_m peaks at 220/340 nm and 280/350 nm regions representing polypeptide backbone and tryptophan (Trp) and tyrosine (Tyr) residues, respectively. HA showed 350-520/350-520 peaks (mixtures both at pH 4 and pH 7. The HA-BSA mixture at both pHs showed fluorescence quenching of BSA. In all the samples 10 mg /L concentration of C is maintained.

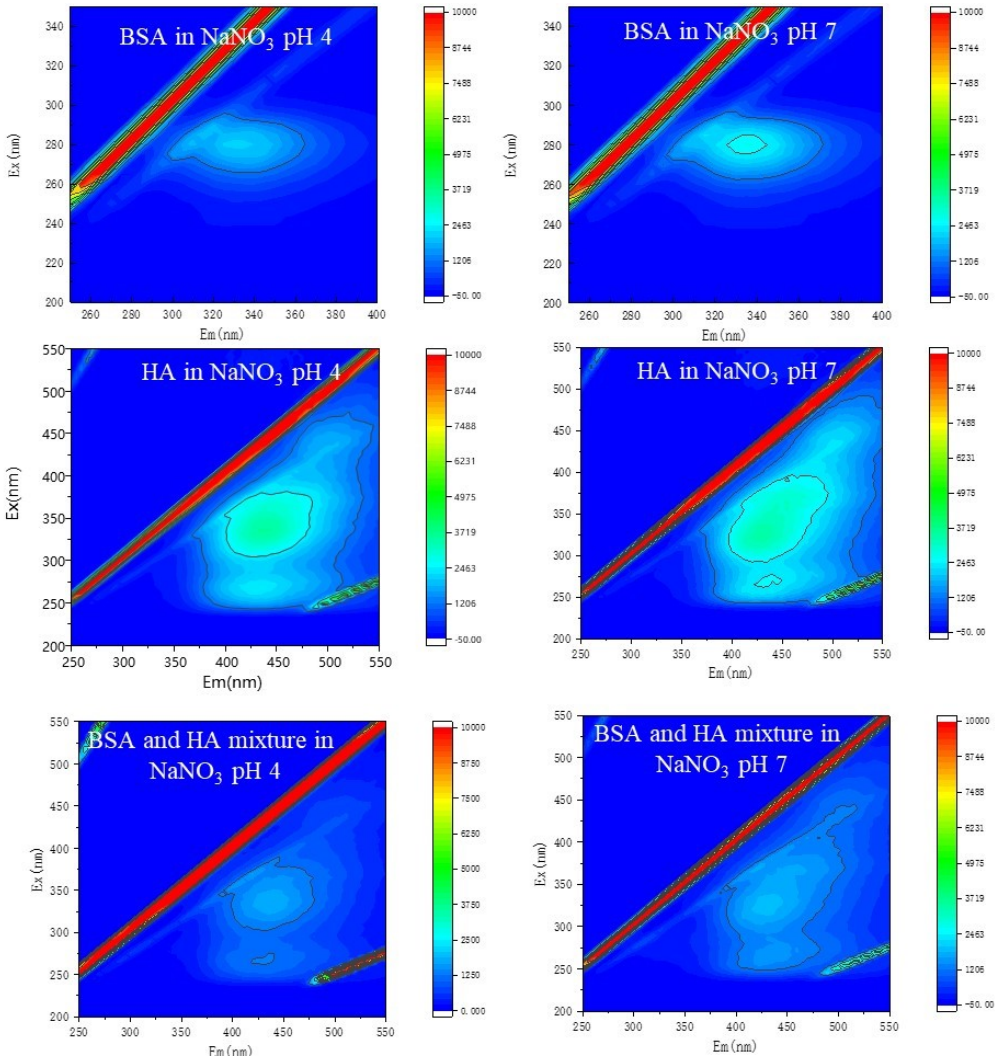

Figure S5. 3DEFM data of BSA, HA, and BSA-HA mixture (10 mg C/L) at pH 4 and pH 7 and in the presence of 10 mM NO_3^-. In addition to the HA-assisted fluorescence quenching of BSA, the binding of weakly hydrated NO_3^- further supplemented the fluorescence quenching of BSA.

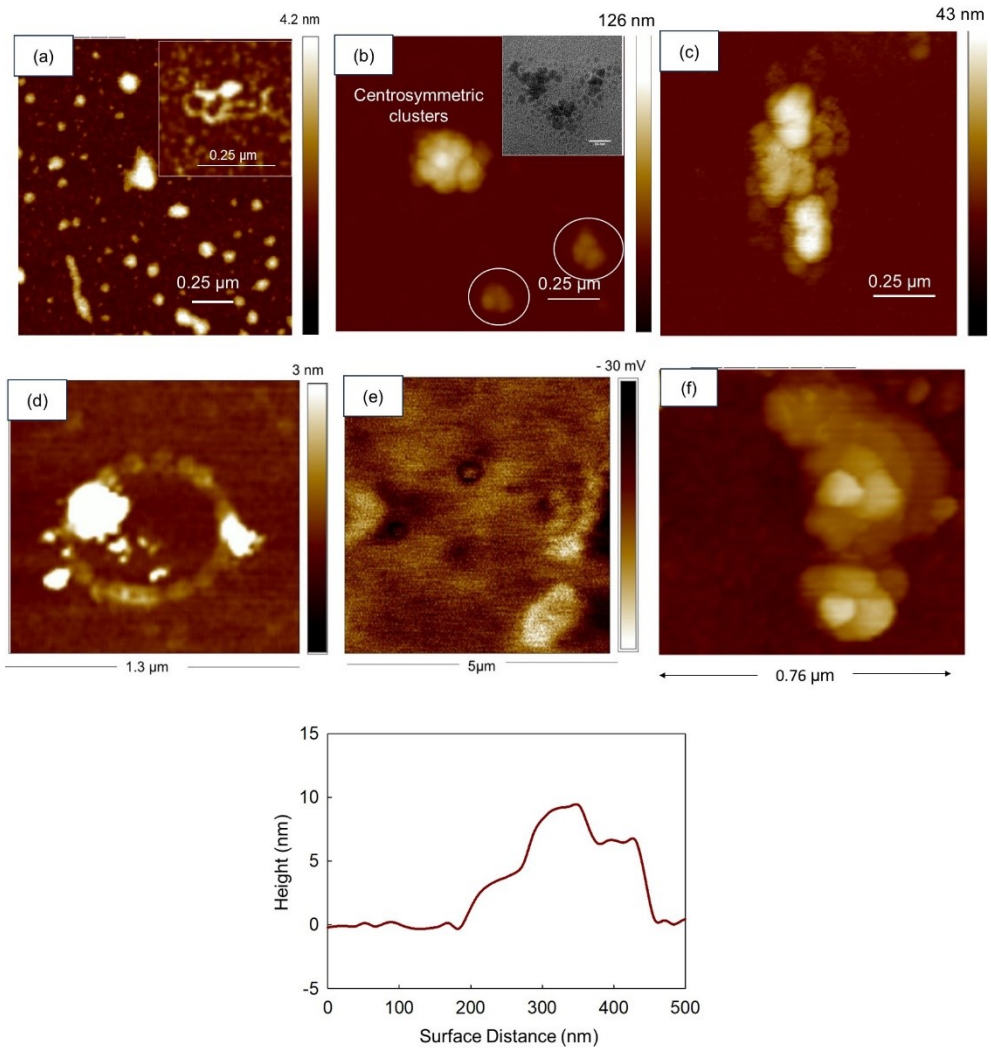

Figure S6. In situ AFM height of the 1:1 binary mixture B-GFeNPs and H-GFeNPs at pH 4 produced (a-c) centrosymmetric aggregate and helical structure. The TEM image in the inset of (b) also showed triskelion-like nanostructure produced from π-π interactions. (d) The same mixture in the presence of 100 mM NO_3^- produced open ring nanoclusters. (e) Ex situ KPFM image of the binary also corroborated the growth of smaller open core toroidal structures at the early stages of screw dislocation-driven growth. (f) Ex situ AFM height image of the binary mixture in 100 mM of NO_3^- also confirmed screw dislocation driven growth of colloidal clusters.

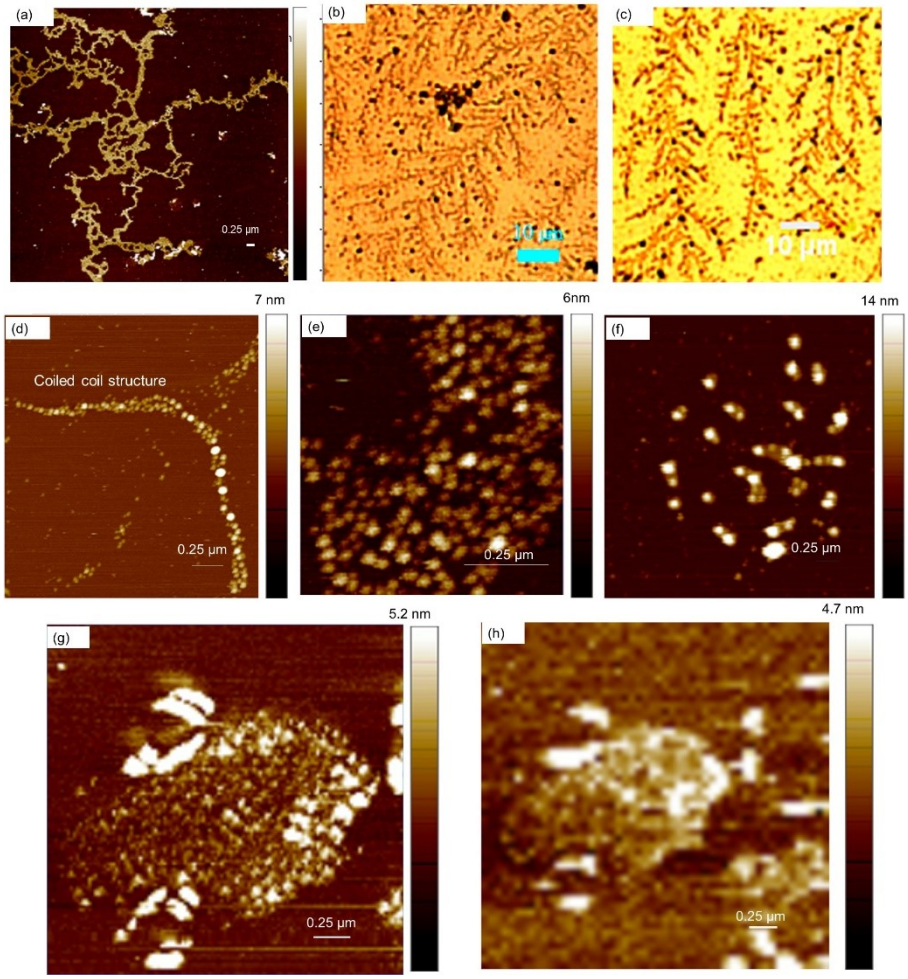

Figure S7. In situ AFM height of the binary mixture B-GFeNPs and H-GFeNPs at pH 7 (a) and optical microscopy of the binary mixture (b-c) showed dendritic structures. But in the presence of 10 mM NO_3^- produced (d) coiled coil structures (e) the growth of dendritic structures and (f) the growth of nanoscale larger crystallites. (d-e) The packing of the colloidal crystal and growth of cubic lattice are shown.

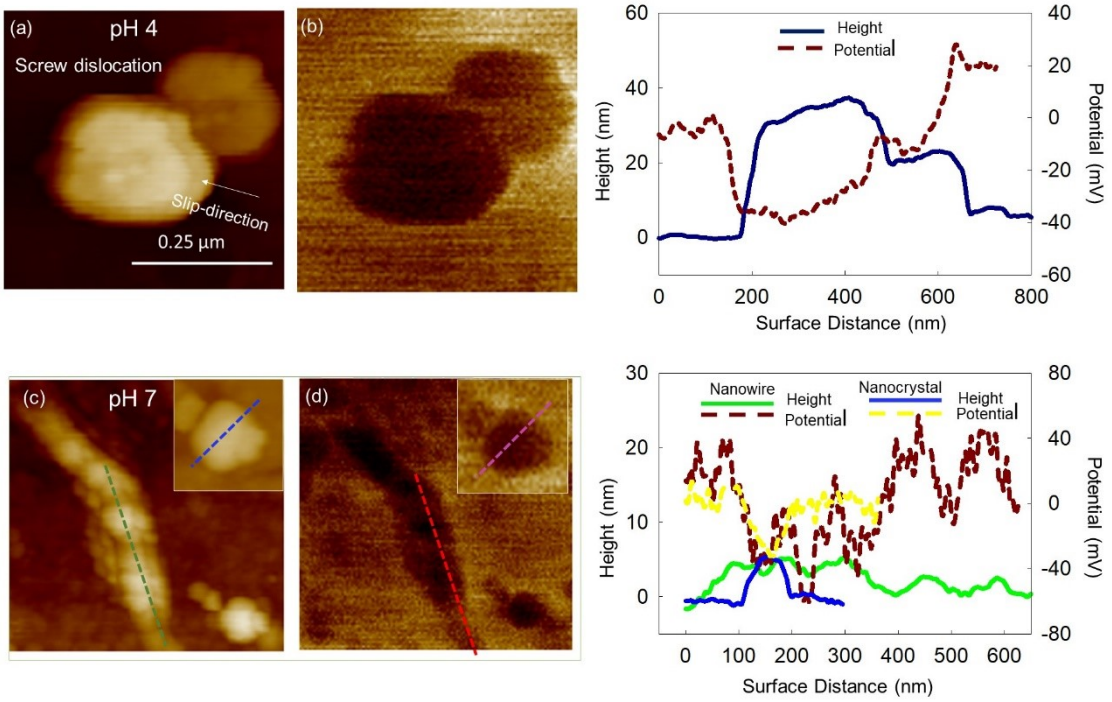

Figure S8. The KPFM (a) height and (b) potential images of the nanowire and individual nanocrystals (insets) at pH 7 revealed crystallization via oriented attachment of TO nanocrystals. But, at pH 4, screw dislocation facilitated the growth of colloidal crystals with (c) platelet-like geometry and layered growth, and (d) the variation in the distribution of surface charge between platelets.

AFM topography and KPFM images of the crystallites produced at pH 4 in the presence of 100 mM NO_3^- corroborated screw dislocation-driven growth with indicated slip movement (Figure S8a and b). KPFM images of the binary mixture at pH 7 in the presence of 10 mM of NO_3^- also exhibited the growth of wire- like colloidal crystals. Although individual nanocrystals shown in the inset had negatively charged core domains, enhanced hydrophobicity and subsequent rise in van der Waals interactions possibly led to crystal growth along the long axis forming dendritic-wire structure.

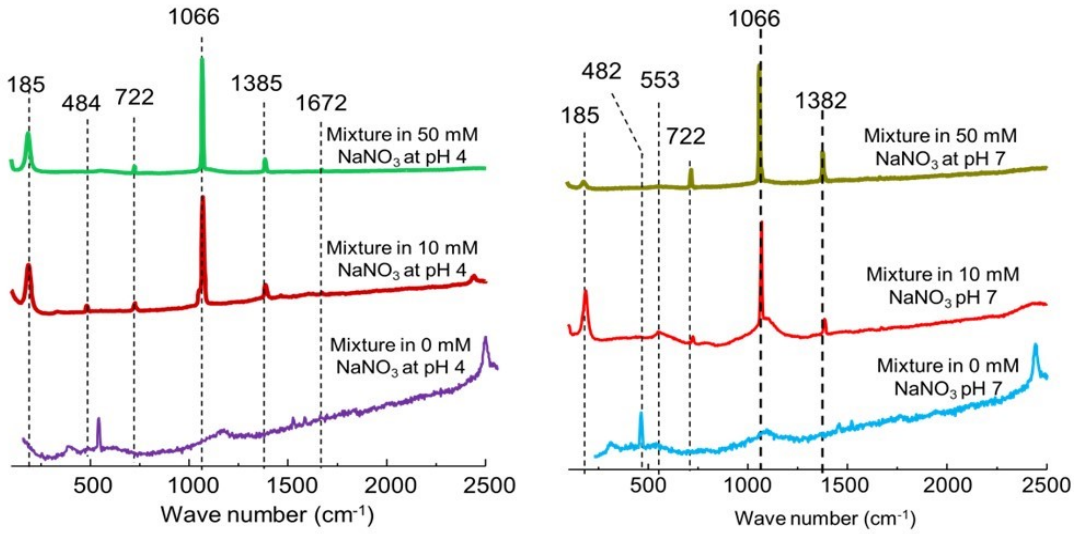

Figure S9. Raman spectra of colloidal crystals produced from the 1:1 binary mixture of B-GFeNPs and H-GFeNPs, both at pH 4 and pH 7 in the presence of 10 mM and 50 mM of NO_3^-, revealed enhanced crystallinity of the colloidal crystals with increasing levels of nitrate.

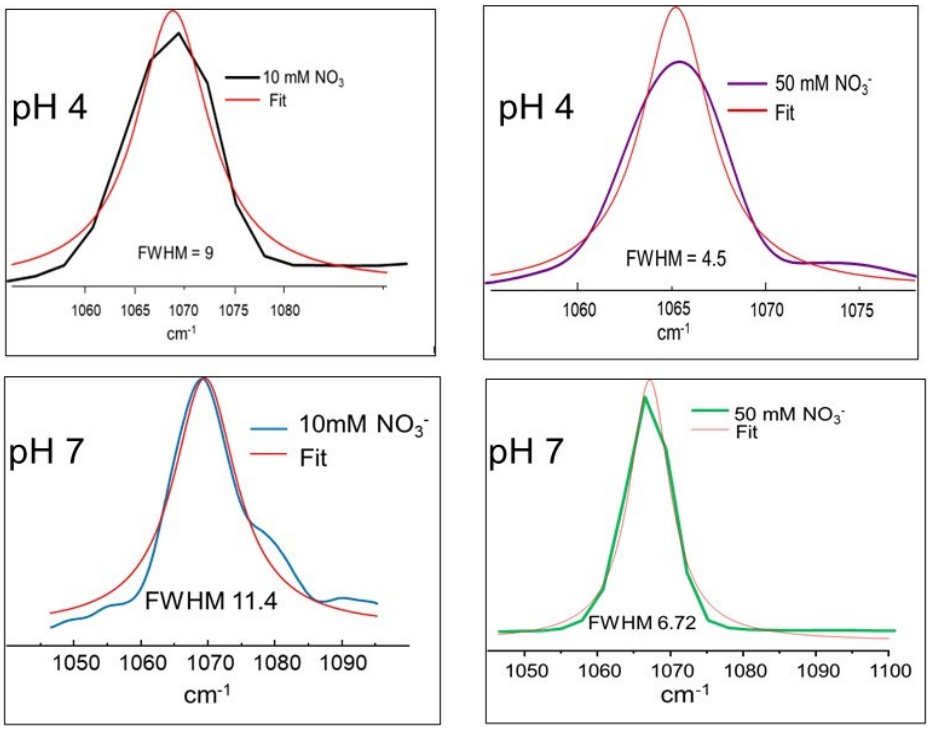

Figure S10. Lorentzian peak fitting of the highest Raman bands at 1066 cm^{-1}, and calculated FWHM values. It is evident that in both the pHs higher concentration of NO_3^- improved the crystallinity of the colloidal crystals produced from the binary mixture of B-GFeNPs and H-GFeNPs.

References

1. S. Li, Z. Peng and R. M. Leblanc, A simple method to determine protein concentration in the protein-nanoparticle conjugates aqueous solution using circular dichroism spectroscopy, *Anal. Chem.*, 2015, 87, 13, 6455–6459.
2. Cz. Ślusarczyk, B. Fryczkowska, M. Sieradzka and J. Janicki, Small-angle X-ray scattering studies of pore structure in cellulose membranes, *Acta. Phys. Polonica A*, 2016, 129, 229-232.
3. S. Ghosh, N. R. Pradhan, H. Mashayekhi, S. Dickert, R. Thantirige, M. T. Tuominen, T. Shu and B. Xing, Binary Short-Range Colloidal assembly of magnetic iron oxides nanoparticles and fullerene (nC_{60}) in natural aquatic medium and air-water interface, *Environ. Sci. Technol.*, 2014, 48, 12285-12291.
4. S. Ghosh, W. Jiang, J. D. McClements and B. Xing, Colloidal stability of magnetic iron

oxide nanoparticles: influence of natural organic matter and synthetic polyelectrolytes, *Langmuir*, 2011, 27, 8036–8043.

5. A. Baral, L. Satish, D. P. Das, H. Sahoo and M. K. Ghosh, Construing the interactions between MnO_2 nanoparticle and bovine serum albumin: insight into the structure and stability of a protein–nanoparticle complex, *New J. Chem*., 2017,41, 8130-8139.

6. U. Anand, C. Jash and S. Mukherjee, Protein unfolding and subsequent refolding: a spectroscopic investigation, *Phys. Chem. Chem. Phys*., 2011, 13, 20418–20426.
7. J. Thøgersen, J. Réhault, M. Odelius, T. Ogden, N. K. Jena, S. J. Knak Jensen, S. R. Keiding and J. Helbing, Hydration dynamics of aqueous nitrate, *J. Phys. Chem. B*, 2013, 117, 12, 3376 –3388.
8. G. Salvi, P. De Los Rios and M. Vendruscolo, Effective interactions between chaotropic agents and proteins, *Proteins: Struc., Func., and Bioinf.*, 2005, 61, 492–499.